The Astrophysical Journal, 634:947–954, 2005 December 1

A VERY HIGH ENERGY GAMMA-RAY SPECTRUM OF 1ES 2344+514

M. Schroedter,[1,2] H. M. Badran,[3] J. H. Buckley,[4] J. Bussons Gordo,[5] D. A. Carter-Lewis,[2] C. Duke,[6] D. J. Fegan,[7] S. F. Fegan,[8] J. P. Finley,[9] G. H. Gillanders,[10] J. Grube,[11] D. Horan,[1] G. E. Kenny,[10] M. Kertzman,[12] K. Kosack,[4] F. Krennrich,[2] D. B. Kieda,[13] J. Kildea,[14] M. J. Lang,[9] Kuen Lee,[4] P. Moriarty,[15] J. Quinn,[7] M. Quinn,[15] B. Power-Mooney,[7] G. H. Sembroski,[9] S. P. Wakely,[16] V. V. Vassiliev,[8] T. C. Weekes,[1] and J. Zweerink[8]

Received 2005 June 1; accepted 2005 July 28

ABSTRACT

The BL Lacertae (BL Lac) object 1ES 2344+514 (1ES 2344), at a redshift of 0.044, was discovered as a source of very high energy (VHE) gamma rays by the Whipple collaboration in 1995 (Catanese et al.). This detection was recently confirmed by the HEGRA collaboration (Tluczykont et al.). As is typical for high-frequency–peaked blazars, the VHE gamma-ray emission is highly variable. On the night of 1995 December 20, a gamma-ray flare of 5.3 σ significance was detected, the brightest outburst from this object to date. The emission region is compatible with a point source. The spectrum between 0.8 and 12.6 TeV can be described by a power law,

$$\frac{d^3N}{dE\,dA\,dt} = (5.1 \pm 1.0_{\rm st} \pm 1.2_{\rm sy}) \times 10^{-7} (E/{\rm TeV})^{-2.54 \pm 0.17_{\rm st} \pm 0.07_{\rm sy}}\ {\rm TeV}^{-1}\ {\rm m}^{-2}\ {\rm s}^{-1}.$$

If we compare the spectral index with that of the other five confirmed TeV blazars, the spectrum of 1ES 2344 is similar to that of 1ES 1959+650, which is located at almost the same distance. The spectrum of 1ES 2344 is steeper than the brightest flare spectra of Markarian 421 (Mrk 421) and Markarian 501 (Mrk 501), both of which are located at a distance about two-thirds that of 1ES 2344, and harder than the spectra of PKS 2155−304 and H1426+428, which are located almost 3 times as far away. This trend is consistent with attenuation caused by the infrared extragalactic background radiation.

Subject headings: BL Lacertae objects: individual (1ES 2344+514) — gamma rays: observations

Online material: color figures

1. INTRODUCTION

To date, the only confirmed extragalactic gamma-ray sources at energies >100 GeV (very high energy; VHE) are BL Lacertae (BL Lac) objects and the giant radio galaxy M87 (Beilicke et al. 2005). BL Lac objects are active galactic nuclei (AGNs) with (1) characteristic radio/optical/X-ray flux, (2) the absence of emission lines with observed equivalent width greater than 5 Å, and (3) a Ca II "break strength" smaller than 25% (Perlman et al. 1996). These criteria define an object with strong nonthermal emission that almost completely masks the thermal emission from the surrounding host galaxy. The spectrum, in a νF_ν representation, shows a double-peaked structure. The only type of BL Lac objects detected so far to emit VHE emission are high-frequency peaked. For these objects, the low-energy component peaks in the soft to hard X-ray regime and the high-energy component peaks in the VHE regime. The six confirmed VHE BL Lac objects are Mrk 421 (Punch et al. 1992; Petry et al. 1996), Mrk 501 (Quinn et al. 1996; Bradbury et al. 1997), 1ES 2344+ 514 (Catanese et al. 1998; Tluczykont et al. 2003), 1ES 1959+ 650 (Nishiyama et al. 1999; Holder et al. 2003; Aharonian et al. 2003), PKS 2155−304 (Chadwick et al. 1999; Aharonian et al. 2005), and H1426+428 (Horan et al. 2002; Aharonian et al. 2002a). The emission level around the two peaks is highly variable, and changes in the spectral shape with flux level have been measured for Mrk 421 (Krennrich et al. 2002, 2003; Aharonian et al. 2002b), Mrk 501 (Djannati-Atai et al. 1999; Aharonian et al. 2001), and 1ES 1959+650 (Aharonian et al. 2003). For the other three BL Lac objects, variations of the spectral shape with flux level have neither been established nor ruled out.

The VHE observations reported here were carried out by the Very Energetic Radiation Imaging Telescope Array System (VERITAS; previously Whipple Gamma Ray) collaboration using an imaging atmospheric Cerenkov telescope (Weekes et al. 1989). The telescope, of 10 m diameter, is located on Mount Hopkins at an altitude of 2320 m above sea level. At the time of

[1] Whipple Observatory, Harvard-Smithsonian Center for Astrophysics, P.O. Box 6369, Amado, AZ 85645-0097.
[2] Department of Physics and Astronomy, Iowa State University, Ames, IA 50011-3160.
[3] Department of Physics, Faculty of Science, Tanta University, Tanta 31527, Egypt.
[4] Department of Physics, Washington University, St. Louis, MO 63130.
[5] Instituto de Fisica de Cantabria (CSIC-UC), Avenida de los Castros s/n, 39005 Santander, Spain.
[6] Department of Physics, Grinnell College, Grinnell, IA 50112-1690.
[7] Department of Experimental Physics, National University of Ireland, Belfield, Dublin 4, Ireland.
[8] Department of Physics and Astronomy, University of California, Los Angeles, CA 90095-1547.
[9] Department of Physics, Purdue University, West Lafayette, IN 47907.
[10] Department of Physics, National University of Ireland, Galway, Ireland.
[11] School of Physics and Astronomy, University of Leeds, Leeds, LS2 9JT, UK.
[12] Department of Physics and Astronomy, DePauw University, Greencastle, IN 46135-0037.
[13] Department of Physics, University of Utah, Salt Lake City, UT 84112.
[14] Department of Physics, McGill University, Montreal, QC H3A 2T8, Canada.
[15] Department of Physical and Life Sciences, Galway-Mayo Institute of Technology, Dublin Road, Galway, Ireland.
[16] Enrico Fermi Institute, University of Chicago, Chicago, IL 60637.

observations, the imaging camera consisted of 109 photomultiplier tubes, each viewing 0°.259 of the sky and arranged in a close-packed hexagonal pattern. The telescope and the data acquisition are described in Cawley et al. (1990).

The organization of this paper is as follows. The status of observations on 1ES 2344 is summarized in § 2. The VHE data and analysis techniques are presented in § 3. This is followed in § 4 by a description of the gamma-ray simulations necessary for the spectral reconstruction, including estimation of the gamma-ray energy in § 4.1. The measured VHE spectra are presented in § 5 and are briefly discussed and summarized in § 6.

2. OBSERVATIONAL STATUS OF 1ES 2344+514

The BL Lac object 1ES 2344+514, at a redshift of 0.044, was detected in the *Einstein* Slew Survey (Elvis et al. 1992) in the energy range 0.2–4 keV. The survey was constructed from data collected during the *High Energy Astronomical Observatory 2* (*HEAO 2*) mission from 1978 to 1981. 1ES 2344 was identified as a BL Lac object in Perlman et al. (1996). The noncontemporaneous spectral energy distribution of 1ES 2344 is shown in Figure 1. Observations at all wavelengths show 1ES 2344 to be an unresolved point source. The central black hole mass is $10^{8.80\pm0.16}\,M_{\odot}$, derived from stellar velocity dispersion measurements (Barth et al. 2003). In the optical regime, a point source with an underlying elliptical host galaxy can be fitted with a radius (half-width at half-maximum) of $r_e = 7.12 \pm 0.02$ kpc ($H_0 = 50$ km s^{-1} Mpc^{-1} and $q_0 = 0$; Urry et al. 2000).

The optical and far-infrared emission from 1ES 2344 contains significant contributions from the host galaxy. The total photometry by the Two Micron All Sky Survey (2MASS; Jarrett et al. 2003) and by the *Hubble Space Telescope* (*HST*; Urry et al. 2000), labeled "Galaxy light" in Figure 1, lies well above the value expected from pure synchrotron emission in the jet. Observations with the *HST* in 1996 measured a *R*-band brightness of the nucleus of 16.83 ± 0.05 mag from a fit of a point source plus galaxy convolved with the point-spread function of the telescope (Urry et al. 2000). During continued monitoring through 1998, the *R*-band brightness varied between 16.47 mag (Nilsson et al. 1999) and 17.00 mag (Falomo & Kotilainen 1999), indicating optical variability. An optical monitoring program in 2000/2001 by Xie et al. (2002) found short-timescale variability to be weak, with maximum intraday variability of $\Delta V = 0.18$ mag and $\Delta R = 0.1$, including galaxy light. A relatively large brightness decrease of 0.35 mag was observed in the *V* band over 2 weeks in 2001 January.

1ES 2344 showed X-ray variability on the timescale of a few hours in the 0.1–10 keV energy band during a week-long campaign in 1996 using the *BeppoSAX* satellite (Giommi et al. 2000). A follow-up observation in 1998 found 1ES 2344 to be in a very low state, implying a frequency shift by a factor of 30 or more of the peak synchrotron emission. Giommi et al. suggested the interpretation that two distinct electron populations contribute to the synchrotron emission: one a steady low-energy component, and the other producing soft to hard X-rays with rapid time variability.

1ES 2344 has been monitored by the Whipple collaboration since 1995 (Catanese et al. 1998). Recently, the High Energy Gamma Ray Astronomy (HEGRA) collaboration reported an independent confirmation of this source (Tluczykont et al. 2003). On the night of 1996 December 5, Whipple VHE and *BeppoSAX* X-ray observations overlapped for 28 minutes, for which we show the X-ray spectrum and VHE flux upper limit in Figure 1. The 99.9% VHE flux upper limit at energies >350 GeV was calculated as in Catanese et al. (1998).

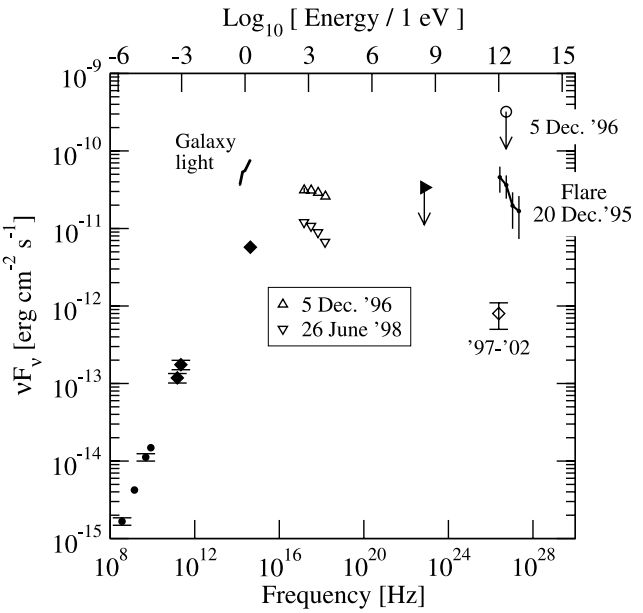

FIG. 1.—Spectral energy distribution of 1ES 2344 along with the VHE flare spectrum obtained with the Whipple 10 m telescope (*line with error bars*). Also shown is the VHE flux upper limit for the night of 1996 December 5 (*open circle*). Other data were taken from the following sources: 365 MHz data from the Texas radio survey (*filled circle*; Douglas et al. 1996), 1.4 GHz data from Green Bank (*filled circle*; White & Becker 1992), 4.85 GHz data from Green Bank (*filled circle*; Gregory & Condon 1991), 8.4 GHz data from the Very Large Array (VLA; *filled circle*; Patnaik et al. 1992), galaxy photometry at millimeter wavelength (*filled diamonds with error bars*; Stevens & Gear 1999), galaxy photometry at the *K*, *H*, and *J* bands from 2MASS (*line segment*; Jarrett et al. 2003), galaxy and nucleus *R*-band photometry obtained with the *Hubble Space Telescope* and corrected for interstellar reddening (*filled diamond*; Urry et al. 2000), X-ray observation with *BeppoSAX* (*see legend*) from Giommi et al. (2000), upper limit at 300 MeV from EGRET (*filled triangle*; Hartman et al. 1999), and quiescent VHE gamma-ray flux during the period 1997–2002 from HEGRA (*open diamond*; Tluczykont et al. 2003).

In the VHE band, the object was observed in a flaring state during the night of 1995 December 20, with a significance of 5.3 σ, the strongest gamma-ray flare measured from this object to date. The quiescent flux level of 1ES 2344, compared to the flare presented here, is about 50 times lower (Tluczykont et al. 2003). The detection of VHE gamma rays from 1ES 2344 in 1995 December, reported by the Whipple collaboration at the 1997 International Cosmic Ray Conference (Catanese et al. 1997), was considered tentative because follow-up observations by this and other VHE observatories through 1997 did not detect further evidence for gamma-ray emission. Monitoring by the Whipple collaboration from 1998 to 2000, however, showed again a small positive excess (Badran 2001). A summary of all published VHE observations of this source is given in Table 1. An initial measurement of the VHE gamma-ray spectrum covering the entire 1995/1996 observing season yielded a spectrum of $(1.14 \pm 0.50) \times 10^{-7} E^{-2.29\pm0.43}$ TeV^{-1} m^{-2} s^{-1}, statistical error only, over the energy range 0.5 TeV $< E <$ 5.0 TeV with χ^2/dof = 3.2/2 (Bussons Gordo 1998a, 1998b).

In Figure 2, we show the two-dimensional gamma-ray sky map during the flare. The gamma-ray map was constructed from a partial data set, referred to as "B" in § 4. The emission region is compatible with a point source. This was determined using a Monte Carlo simulation of the telescope response to a point source of gamma rays. A small telescope pointing error of less than 0°.05 may have been present during the observations, but due to the lack of bright stars in the field of view, we are not able to determine this in retrospect. The centroid of the measured gamma-ray

TABLE 1
SUMMARY OF VHE MEASUREMENTS OF 1ES 2344

Date	Exposure (hr)	S[a] (σ)	Integral Flux ($\times 10^{-7}$ m^{-2} s^{-1})	$E_{\rm thresh}$ (TeV)	Reference
1995/1996	20.5	5.8	1.7 ± 0.5	0.35	1
1995 Dec 20	1.85	5.3[b]	6.6 ± 1.9	0.35	1
1996/1997	24.9	0.4	<0.82[c]	0.35	1
1997 Dec	15.8	NA	<0.29[d]	1.0	2
1997–2002	72.5	4.4	0.08 ± 0.03	0.8	3
1998	23.8	3.3[b]	<0.09[d]	1.0	4
2000	3.1	2.4	1.1 ± 0.1[e]	$\approx$0.4	5

[a] Statistical excess.
[b] Part of the data listed in the row above.
[c] 99.9% C.L. upper limit.
[d] 99% C.L. upper limit.
[e] Statistical error only.
REFERENCES.— (1) Catanese et al. 1998; (2) Aharonian et al. 2000; (3) Tluczykont et al. 2003; (4) Konopelko et al. 1999; (5) Badran 2001.

emission is displaced from the known location of 1ES 2344 by $0^{\circ}.02 \pm 0^{\circ}.02$ in right ascension and $0^{\circ}.03 \pm 0^{\circ}.02$ in declination. A conservatively estimated $0^{\circ}.1$ circle of confusion contains three galaxies and two radio sources, but no other X-ray sources. Thus, the gamma-ray emission likely originated from 1ES 2344.

The EGRET 95% confidence level upper limit for 1ES 2344 is 6.98×10^{-8} counts cm^{-2} s^{-1}, $E > 100$ MeV (Hartman et al. 1999). The peak response for most sources detected with EGRET lies at around 300 MeV, which corresponds to an upper limit at 300 MeV of about 3.4×10^{-11} ergs cm^{-2}.

3. GAMMA-RAY FLARE AND BACKGROUND DATA

Observations with the 10 m telescope were carried out in two pointing modes: (1) with the source in the center of the field of view (ON observation) and (2) with the telescope pointing offset from the source direction by 30$^{\rm m}$ in right ascension, called the OFF observation. The OFF observation is a measurement of the background caused by cosmic rays. On the night of 1995 December 20, four ON observations were taken with a combined exposure time of 110 minutes. The last ON observation during the night was not complemented with an OFF observation, as is necessary for spectral measurements. Therefore, an OFF observation was selected from the 1995/1996 season on the basis of its similarity to the ON observation in elevation, cosmic-ray rate, and night-sky brightness. For each ON observation, Table 2 lists the UTC start time, the average observing elevation, the throughput factor for both the ON and OFF observations, and the measured gamma-ray rate. The throughput factor measures the cosmic-ray rate relative to a reference observation taken under clear skies (LeBohec & Holder 2003). The weather during these observations was rated "A" by the observers, indicating clear skies. Figure 3 confirms this by comparing these observations with other "A" weather observations taken between 1995 October and 1996 April.

TABLE 2
DETAILS OF THE OBSERVATIONS TAKEN ON 1995 DECEMBER 20

UTC[a]	Elevation	Throughput[b]	Gamma-Ray Rate[c]
2:32	64°	$0.77/0.78 \pm 0.08$	0.70 ± 0.28
3:34	55°	$0.68/0.71 \pm 0.08$	1.04 ± 0.37
4:35	47°	$0.52/0.57 \pm 0.05$	0.91 ± 0.42
5:36	37°/36°	$0.45/0.41 \pm 0.04$	1.54 ± 0.47
Average			1.14 ± 0.20

[a] Start time of the ON observation. The first three ON observations lasted for 28 minutes followed by an OFF observation. The last observation had a length of only 10 min. A complementary OFF observation, necessary for the spectral analysis, was chosen on the basis of similar observation conditions.
[b] Relative cosmic-ray rate for ON/OFF observations; see text.
[c] Gamma-ray rate per minute after applying Supercuts95 (Catanese et al. 1998).

The standard analysis method for data taken with the 10 m telescope (Reynolds et al. 1993) includes conditioning of the images, parameterization, and selection of gamma-ray–like events.

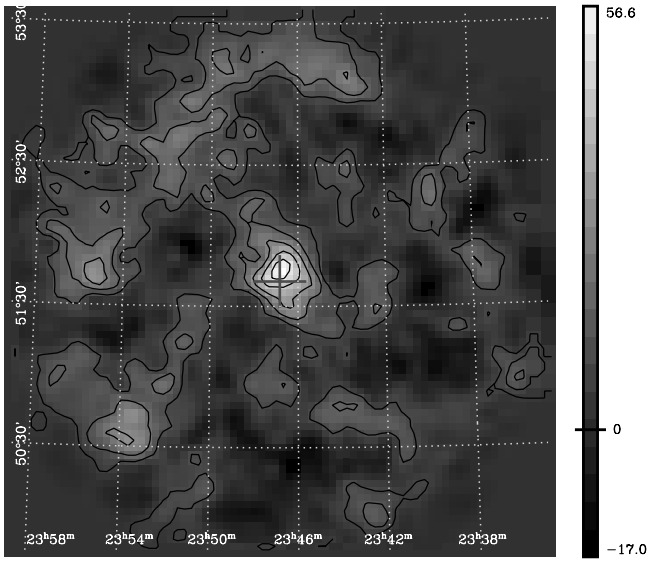

FIG. 2.—Gamma-ray sky map of the field of view around 1ES 2344, with position indicated by the dark gray plus sign. The colors show excess counts with overlaid significance contours in steps of 1 standard deviation per contour. The dotted lines show the right ascension and declination. [*See the electronic edition of the Journal for a color version of this figure.*]

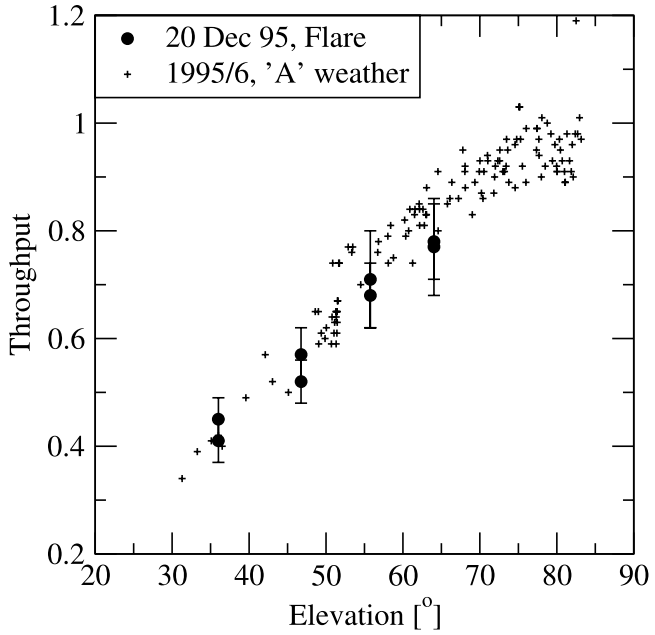

FIG. 3.—Relative cosmic-ray rate of 1ES 2344 flare data compared to observations carried out under clear skies (rated "A" by observers) in 1995/1996. For clarity, the error bars are only shown for the flare data.

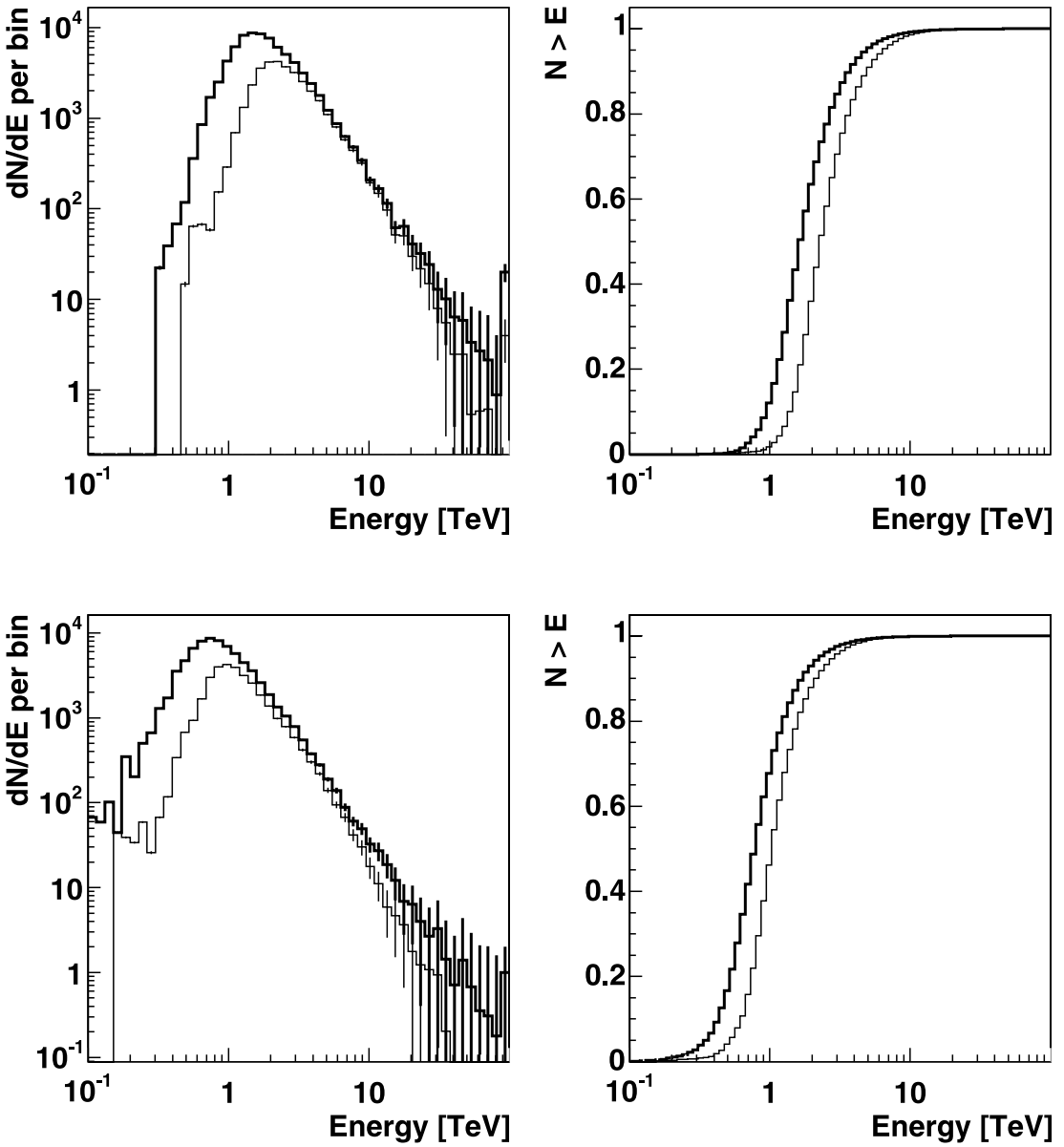

FIG. 4.—Simulated trigger rate at 41° elevation (*left*) and 58° (*right*) of gamma rays distributed with a power-law index of −2.5. The two lines show the rate after the application of spectral cuts (*thick lines*) and Supercuts95 (*thin lines*).

Conditioning of the images consists of (1) flat fielding of the relative gain between pixels, (2) equalizing the sky brightness between the ON and OFF observations (Cawley 1993), and (3) removing pixels that are below a certain signal-to-noise ratio. Images are then parameterized by their rms width and length, their distance from the center of the field of view (Hillas 1985), and the orientation angle of their major axis relative to the pointing direction of the telescope, α (Weekes et al. 1987). The total amount of light collected is referred to as the size of the image and is measured in digital counts (dc).

The gamma-ray signal is derived from the excess number of events between ON and OFF runs, where only those images are selected that are likely to have been produced by a gamma-ray source located at the center of the field of view. The rate given in Table 2 shows the gamma-ray rate after application of one particular set of selection criteria (cuts) called Supercuts95 (Catanese et al. 1998). These cuts are not optimal for spectral measurements because the selection efficiency for gamma rays decreases dramatically with energy. Therefore, a different set of cuts was developed empirically using simulated gamma-ray events; see § 4.1. The analysis of the data given in Table 2 is in agreement with a previous analysis by Catanese et al. (1998).

4. CALIBRATION AND SPECTRAL RECONSTRUCTION

The data contain a relatively low gamma-ray rate and were taken over a wide range of elevations. To obtain an accurate energy calibration, our analysis technique requires us to analyze different elevation ranges separately. To maintain a good signal-to-noise ratio, the data were combined at the two average elevations of 58° and 41° and are referred to as data sets A and B, respectively. The data in these two sets were taken sequentially during the night, allowing us to investigate time variability in the emission level.

A total of 500,000 gamma-ray–initiated showers were simulated at each elevation; these were randomly distributed in energy according to a power law of index −2.5, covering a circular area around the telescope axis. The Monte Carlo simulations of gamma-ray–initiated particle showers in the atmosphere and subsequent

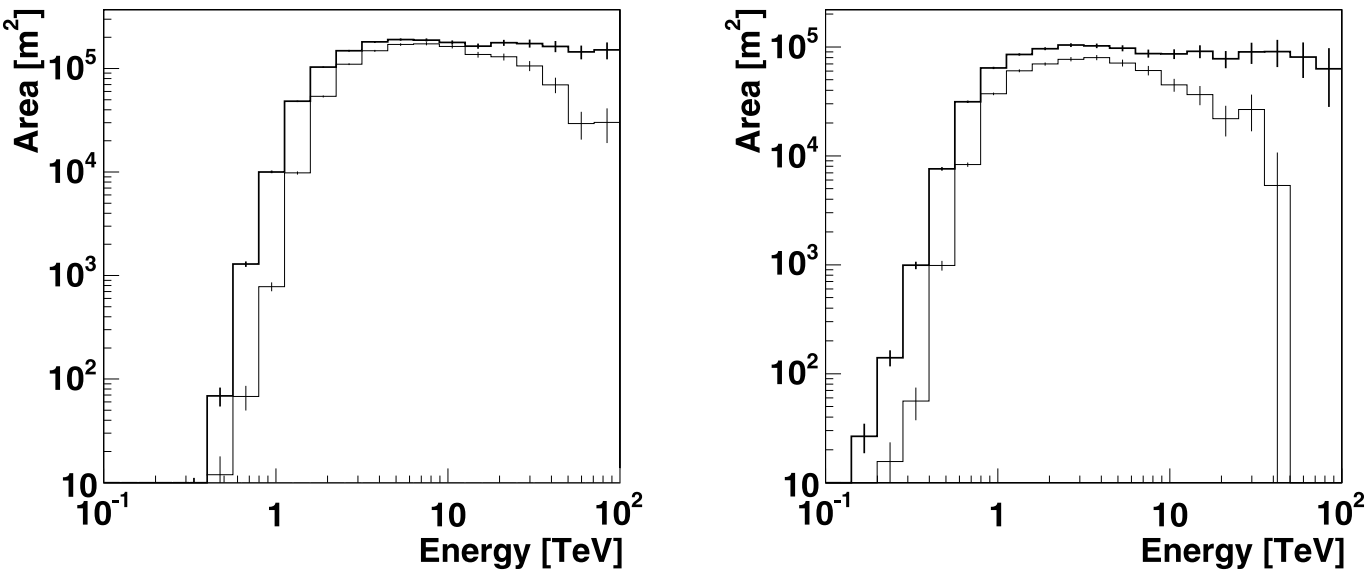

FIG. 5.—Collection area for gamma rays at 41° elevation (*left*) and at 58° elevation (*right*) in 1995 for spectral cuts (*thick line*) and Supercuts95 cuts (*thin line*).

detection of Cerenkov photons by the telescope were carried out with the Grinnell-ISU (GrISU) package.[17] At 58° elevation, simulations were carried out over the energy range 0.1–100 TeV and impact radius less than 300 m. At 41° elevation, simulations were carried out over the energy range 0.3–100 TeV and impact radius less than 350 m. The low-energy cutoff was chosen to extend beyond the range of energies of events that trigger the telescope. The night-sky brightness level of simulated showers was matched to that measured from the data.

The absolute light throughput of the telescope was calibrated with Cerenkov images of muons recorded by the telescope. For this, only complete muon rings were selected using a specially developed algorithm (Schroedter 2004). This ensures that the total amount of light is well known. The light throughput factor derived in this way was used to measure the spectrum of the Crab Nebula during the 1995/1996 season. With statistical (st) and systematic (sy) errors, the spectrum of the Crab Nebula between 0.3 and 13 TeV can be fitted by $(4.2 \pm 0.3_{\rm st} \pm 0.7_{\rm sy}) \times 10^{-7} E^{-2.38\pm0.08_{\rm st}\pm0.04_{\rm sy}}$ TeV^{-1} m^{-2} s^{-1}, with $\chi^2_{\rm min}/{\rm dof} = 3.2/(9-2)$. This is compatible with other measurements (Mohanty et al. 1998; Hillas et al. 1998).

The energy resolution of the spectral analysis depends on rejecting cosmic-ray images and selecting only those gamma-ray images with well-defined image parameters. The collection area near the triggering threshold is difficult to model in the simulations, and hence a software cut on the minimum brightness is applied that lies substantially above the hardware threshold. The following set of loose cuts were then applied to data and simulations: $0.^\circ31 <$ distance $< 1.^\circ1$, length/size < 0.00085 deg dc^{-1}, max$2 > 65$ dc, and $\alpha < 25^\circ$.

The differential trigger rates at 41° elevation, corresponding to data set B, are shown in Figure 4 for a spectrum with a differential index of −2.5. The peak trigger rate occurs at an energy of 1.4 TeV for spectral cuts, described below, and at 2.1 TeV with Supercuts95. With these cuts, 90% of the triggers occur above 1.05 and 1.67 TeV, respectively. The collection area, shown in Figure 5, reaches 10% of its maximum value of 170,000 m^2 at an energy of about 1.1 TeV for spectral cuts. The differential trigger rates at 58° elevation, corresponding to data set A, are also shown in Figure 4. The peak trigger rate occurs at an energy of 0.69 TeV for spectral cuts and 1.1 TeV with Supercuts95. For these two sets of cuts, 90% of the triggers occur above 0.48 and 0.75 TeV, respectively. The collection area, also shown in Figure 5, reaches 10% of its maximum value of 136,000 m^2 at an energy of about 0.51 TeV for spectral cuts.

[17] Available at http://www.physics.utah.edu/gammaray/GrISU/.

4.1. *Event Selection and Energy Estimation*

The spectral analysis method has been described in Petry et al. (2002) and Mohanty et al. (1998). Simulations at 41° elevation show an energy resolution of rms$(\Delta \log E) = 0.15$ or rms$(\Delta E/E) = 0.40$, with an energy estimation bias of $|\Delta \log E| = 0.018$ over the energy region $E = 0.8$–40 TeV. This energy range begins at 10% of the peak collection area. A cutoff at the high energies is necessary, as the limited field of view of the camera truncates large showers and the estimated and true energies begin to diverge. At 58° elevation, the energy resolution is rms$(\Delta \log E) = 0.16$ or rms$(\Delta E/E) = 0.49$, and $|\Delta \log E| = 0.012$ over the energy range $E = 0.4$–25 TeV.

The gamma-ray signal is contaminated by a large fraction of cosmic-ray events. To reject this background, cuts are imposed on the parameters distance, width, length, and α. The cuts derived from the Monte Carlo simulations scale with size so that the efficiency of selecting gamma rays remains unchanged as a function of energy. The fraction of gamma rays passing the cuts for simulations at 41° elevation is 86%, and it is 87% at 58° elevation. The distributions of the parameters width, length, and α are shown for simulated gamma rays in Figure 6. The cuts are chosen at a nominal 2 standard deviations around the mean value. The simulations at 58° are limited by statistics at high energies, making the cuts somewhat inefficient. In particular, the upturn at large dc values of the α-cut is unphysical, but the cut level still remains below the Supercuts95 value of 15°. The unphysical upturn is due to the second-order polynomial used in fitting the cut level. For comparison, the level of Supercuts95 is also shown in Figure 6.

5. FLARE SPECTRA

The number of excess gamma-ray events in each energy bin after application of all cuts is presented for both data sets in Tables 3 and 4. Due to the very small signal, the bin width is

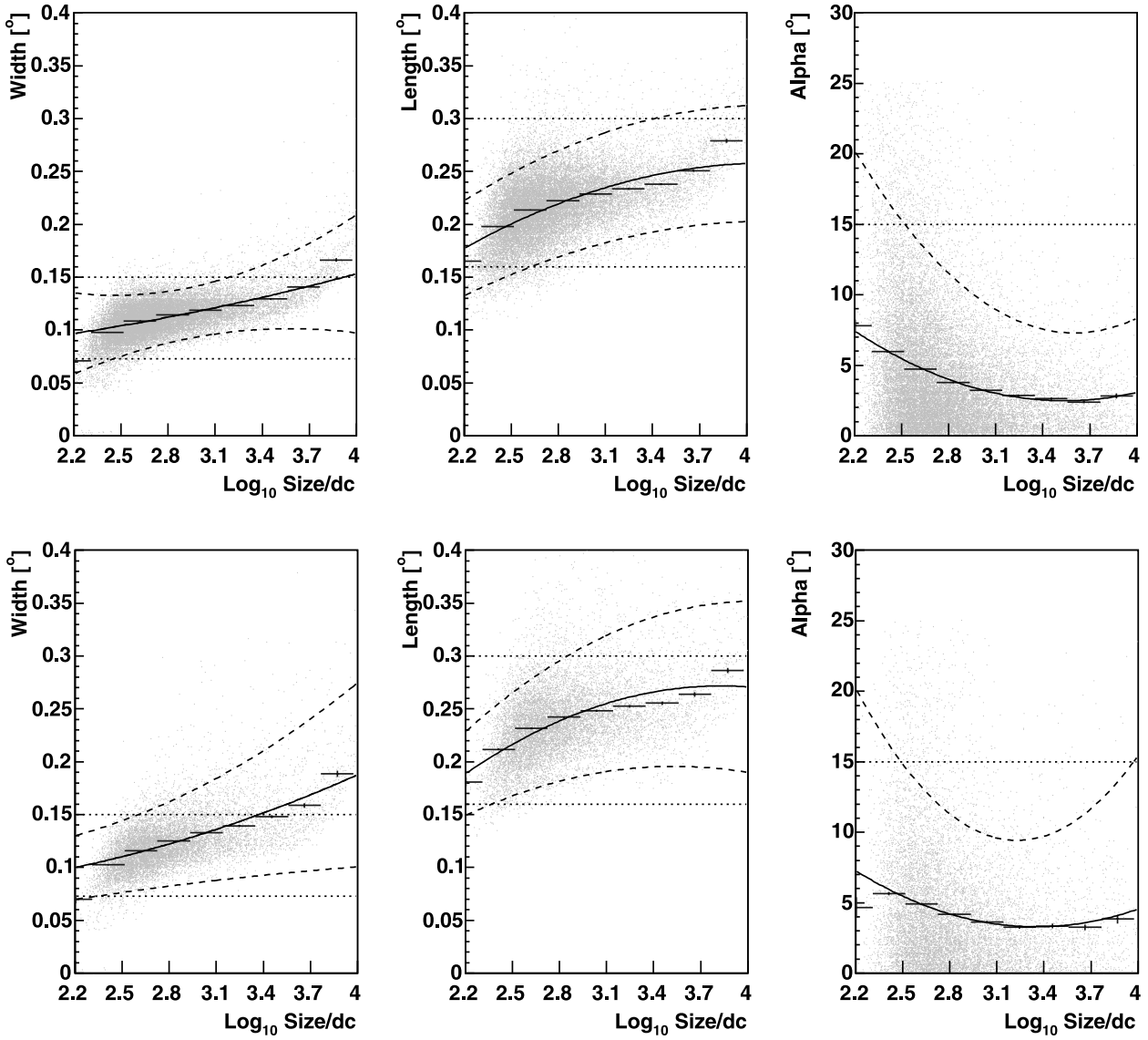

FIG. 6.—Simulated parameter distributions and cut levels with log (size) after application of loose cuts; see text. *Top,* simulated at 41° elevation; *bottom,* 58° elevation. The dots represent simulated events, and crosses represent the average. The solid lines show the fitted polynomial to the average. Dashed lines show the actual cut chosen at a tolerance of 2 standard deviations around the average. Dotted lines show the cut level of Supercuts95. [*See the electronic edition of the Journal for a color version of this figure*.]

TABLE 3

EVENT STATISTICS AND FLUX FOR DATA SET A

Energy (TeV)	ON (events)	OFF (events)	ON−OFF (events)	S (σ)	Flux ($\mathrm{TeV}^{-1}\ \mathrm{m}^{-2}\ \mathrm{s}^{-1}$)
0.56.....	63	38	25 ± 10	2.5	$(1.29 \pm 0.51) \times 10^{-6}$
1.12.....	83	63	20 ± 12	1.7	$(1.27 \pm 0.77) \times 10^{-7}$
2.24.....	39	42	-3 ± 9	−0.3	$<3.91 \times 10^{-8}$
4.47.....	22	19	3 ± 6	0.5	$<1.46 \times 10^{-8}$
8.91.....	8	7	1 ± 4	0.3	$<3.62 \times 10^{-9}$
Total	220	174	44 ± 19.8	2.2	...

NOTE.—Upper limits are given at the 98% confidence level.

TABLE 4

EVENT STATISTICS AND FLUX FOR DATA SET B

Energy (TeV)	ON (events)	OFF (events)	ON−OFF (events)	S (σ)	Flux ($\mathrm{TeV}^{-1}\ \mathrm{m}^{-2}\ \mathrm{s}^{-1}$)
1.12.....	55	30	25 ± 9	2.7	$(3.64 \pm 1.34) \times 10^{-7}$
2.24.....	86	51	35 ± 12	3.0	$(7.24 \pm 2.42) \times 10^{-8}$
4.47.....	35	20	15 ± 7	2.0	$(9.82 \pm 4.85) \times 10^{-9}$
8.91.....	14	6	8 ± 4	1.8	$(2.11 \pm 1.19) \times 10^{-9}$
17.78.....	7	4	3 ± 3	0.9	$<1.19 \times 10^{-9}$
35.48.....	0	2	-2 ± 1	−1.4	$<1.43 \times 10^{-10}$
Total	197	113	84 ± 17.6	4.8	...

NOTE.—Upper limits are given at the 98% confidence level.

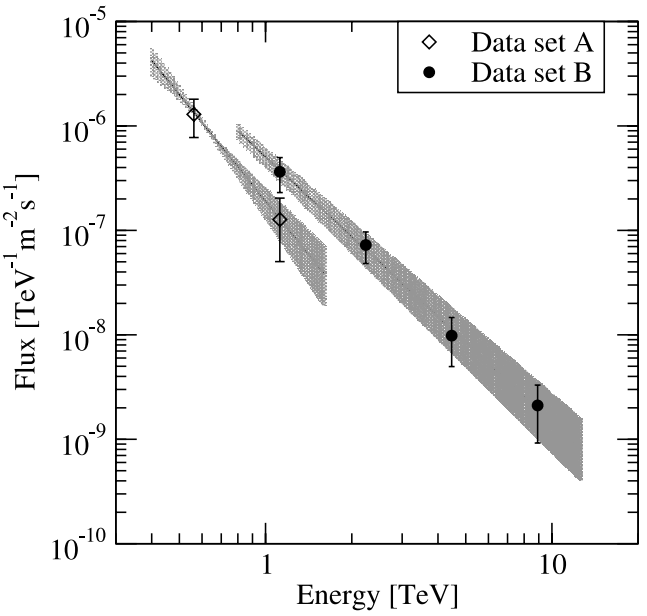

FIG. 7.—Differential flux spectrum of 1ES 2344 on 1995 December 20. Spectra from data sets A (*diamonds*) and B (*circles*) are shown together with power-law fits (*solid lines*). The shaded regions show the confidence interval of the power-law fits and were obtained by varying both parameters to their individual 68% confidence intervals.

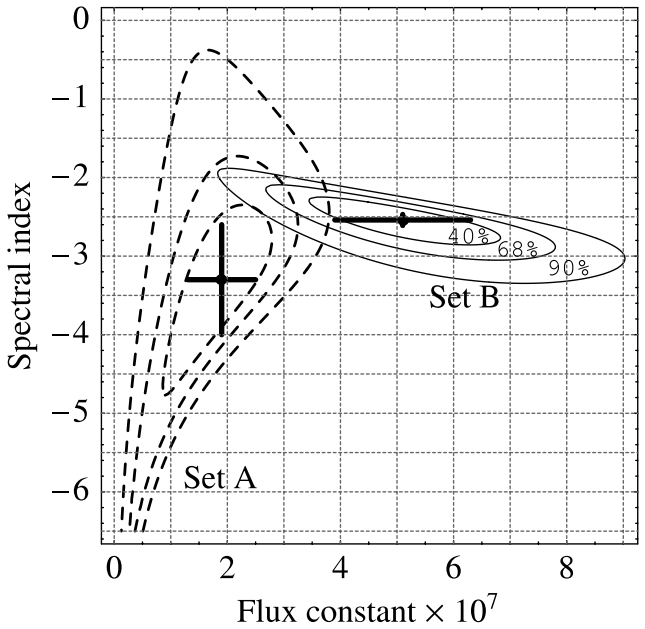

FIG. 8.—Confidence regions corresponding to the spectrum of data set A (*dashed lines*) and set B (*solid lines*). Confidence regions are shown with probability content of 40%, 68%, and 90% for the simultaneous values of the spectral index and flux constant. Also shown are the systematic errors on the flux constant and spectral index (*plus signs*).

chosen at twice the energy resolution $\Delta(\log E) = 0.3$ (Petry et al. 2002). Flux upper limits are given if the gamma-ray significance is less than 1 σ in the energy bin. The upper limits are at the 98% confidence level and are calculated according to the method of Helene (1983).

The spectra for the two data sets A and B are shown in Figure 7. The error bars show the statistical error only.

For data set B, the power-law fit to the spectrum over the energy range from 0.8 to 12.6 TeV is given by

$$\frac{dN}{dE\,dA\,dt} = (5.1 \pm 1.0_{\rm st} \pm 1.2_{\rm sy}) \times 10^{-7} \times (E/\mathrm{TeV})^{-2.54\pm0.17_{\rm st}\pm0.07_{\rm sy}}\ \mathrm{TeV}^{-1}\ \mathrm{m}^{-2}\ \mathrm{s}^{-1}, \quad (1)$$

with $\chi^2_{\rm min}/\mathrm{dof} = 0.2/(4-2)$. The χ^2 probability for this data to randomly arise from the power-law fit is 0.9. The statistical error represents the 68% confidence interval (CI) for a fit with one free parameter while the other parameter is frozen at its optimum value. The 68% CI with two simultaneous free parameters, defined by $\chi^2_{\rm min} + 2.3$, is shown in Figure 8.

The systematic errors of the flux constant and spectral index arising from the energy calibration and the cut tolerance are indicated in Figure 8 by crosses. The cut tolerance, with a nominal value of 2 standard deviations, was varied between 1.5 and 2.5 standard deviations; the level of the muon-based energy calibration is ±10%. The uncertainty in the energy calibration affects mostly the flux constant. For example, a 10% change in the energy calibration changes the flux constant by 25% or 30% if the spectrum has a differential index of −2.5 or −3.0, respectively. In addition, due to the large elevation range covered, a small systematic uncertainty on the order of 10%–15% is intrinsic to the GrISU simulations (Krennrich et al. 1999). The spectral index is mostly affected by varying the cut tolerance. It should be noted that the systematic error evaluated in this way is smaller than the statistical error. This means that a good estimate of the systematic error is not possible with this method; nevertheless, it does indicate the relative importance of the two sources of error.

For data set A, the power-law fit over the energy range from 0.4 to 1.6 TeV is given by

$$\frac{dN}{dE\,dA\,dt} = (1.9 \pm 0.6_{\rm st} \pm 0.6_{\rm sy}) \times 10^{-7} \times (E/\mathrm{TeV})^{-3.3\pm0.7_{\rm st}\pm0.7_{\rm sy}}\ \mathrm{TeV}^{-1}\ \mathrm{m}^{-2}\ \mathrm{s}^{-1}, \quad (2)$$

and the confidence interval contours are shown in Figure 8.

As the spectral indexes of the two spectra are compatible, it is possible to adjust the flux constant of the less significant spectrum (data set A) so that it overlaps, in a least-squares sense, with the spectrum of data set B. However, as the statistical significance of data set A is very small compared to set B, combining the two data sets results in an insignificant improvement in the statistical error of the spectral index. Therefore, the spectral measurement of 1ES 2344 derived here is best represented by the spectrum of data set B alone.

6. DISCUSSION

1ES 2344 is a variable source; during the flare on 1995 December 20, the gamma-ray emission from 1ES 2344 was about 50 times brighter than that during the quiescent phase measured several years later. To obtain an accurate energy calibration, our analysis technique required us to analyze data taken at different observing elevations separately. Therefore, we split the data into two sets, A and B, with 56 and 38 minutes of exposure time, respectively. The data sets were taken consecutively during the night. The spectral indices measured from the two data sets are compatible with each other. The increase of the flux constant over the 2 hr of observation, although also not very significant, is not unexpected, as the very large variability of the VHE flux on a timescale of hours has been observed for other blazars (Gaidos et al. 1996; Quinn et al. 1996; Holder et al. 2003; Aharonian et al. 2005).

The measured VHE spectra are attenuated through pair production with the infrared extragalactic background light (EBL; Nikishov 1962). Due to the EBL spectral shape, the attenuation manifests itself as a steepening of the measured VHE spectrum between roughly 1 and 5 TeV and becomes more pronounced with larger redshift. A cutoff feature is thus expected in the VHE spectra, if variations in the intrinsic VHE spectrum are ignored. Such a cutoff feature has been established for Mrk 421 and Mrk 501 (Aharonian et al. 2001; Krennrich et al. 2001, 2002). Their spectra can be described with a power law with an exponential cutoff: $dN/dE \propto E^{-\alpha} \exp(E/E_0)$. The cutoff energy, E_0, differs between the two blazars by 2.6 ± 1.2 TeV (Aharonian et al. 2002b). Unfortunately, for 1ES 2344 the low statistical significance of the spectrum precludes the measurement of such a cutoff energy.

VHE spectra are now available for all six confirmed TeV blazars. The power-law spectral indexes of fits to the brightest flares from the blazars appear to steepen with redshift (Schroedter 2005). The spectral index of the 1ES 2344 VHE flare is steeper than the brightest flare spectra of Mrk 421 and Mrk 501, both of which are located at about two-thirds the distance of 1ES 2344. The flare spectra of PKS 2155−304 and H1426+428, which are located almost 3 times as far away, are softer than that of 1ES 2344. The spectral index of the 1ES 2344 flare is similar to the flare spectrum of 1ES 1959+650, which is located at almost the same redshift. This trend is consistent with attenuation caused by the infrared extragalactic background radiation (Schroedter 2005; Stecker 1999). Alternatively, galaxy evolution might be responsible for the observed spectral steepening with redshift. For example, if younger galaxies have enhanced mid-infrared radiation nearer to the central black hole, then this would produce gamma-ray attenuation indistinguishable from that caused by the EBL.

No contemporaneous measurements at other wavelengths were taken during the gamma-ray flare of 1ES 2344 on 1995 December 20. This precludes the application of models to constrain the gamma-ray production mechanism, because the gamma-ray emission is known to be highly variable. Almost 1 year later, on 1996 December 5, a simultaneous TeV/X-ray observation occurred together with the *BeppoSAX* satellite. The detailed X-ray spectrum measured during this night (Giommi et al. 2000) is complemented, however, only by an upper limit of the TeV flux, again precluding models to be significantly constrained.

We acknowledge the technical assistance of K. Harris, T. Lappin, and E. Roache. This research has made use of the NASA/IPAC Extragalactic Database (NED), which is operated by the Jet Propulsion Laboratory, California Institute of Technology, under contract with the National Aeronautics and Space Administration.

REFERENCES

Aharonian, F., et al. 2001, ApJ, 546, 898
———. 2002a, A&A, 384, L23
———. 2002b, A&A, 393, 89
———. 2003, A&A, 406, L9
———. 2005, A&A, 430, 865
Aharonian, F. A., et al. 2000, A&A, 353, 847
Badran, H. M. 2001, in AIP Conf. Proc. 587, Gamma 2001: Gamma-Ray Astrophysics, ed. S. Ritz, N. Gehrels, & C. R. Shrader (New York: AIP), 281
Barth, A. J., Ho, L. C., & Sargent, W. L. W. 2003, ApJ, 583, 134
Beilicke, M., et al. 2005, in Proc. 22nd Texas Symp. on Relativistic Astrophysics, ed. P. Chen, E. Bloom, G. Madejski, & V. Patrosian (Stanford: SLAC), in press (astro-ph/0504395)
Bradbury, S. M., et al. 1997, A&A, 320, L5
Bussons Gordo, J. 1998a, Ph.D. thesis, Univ. College Dublin
———. 1998b, in Rayos Cósmicos 98, Proc. 16th European Cosmic Ray Symposium, ed. J. Medina (Alcalá de Henares: Univ. Alcalá), 379
Catanese, M., et al. 1997, in Proc. 25th Int. Cosmic Ray Conf. (Durban), 3, 277
———. 1998, ApJ, 501, 616
Cawley, M. F. 1993, in Towards a Major Cerenkov Detector II, ed. R. C. Lamb (Ames: Iowa State Univ.), 176
Cawley, M. F., et al. 1990, Exp. Astron., 1, 173
Chadwick, P. M., et al. 1999, ApJ, 513, 161
Djannati-Atai, A., et al. 1999, A&A, 350, 17
Douglas, J. N., Bash, F. N., Bozyan, F. A., Torrence, G. W., & Wolfe, C. 1996, AJ, 111, 1945
Elvis, M., Plummer, D., Schachter, J., & Fabbiano, G. 1992, ApJS, 80, 257
Falomo, R., & Kotilainen, J. K. 1999, A&A, 352, 85
Gaidos, J. A., et al. 1996, Nature, 383, 319
Giommi, P., Padovani, P., & Perlman, E. 2000, MNRAS, 317, 743
Gregory, P. C., & Condon, J. J. 1991, ApJS, 75, 1011
Hartman, R. C., et al. 1999, ApJS, 123, 79
Helene, O. 1983, Nucl. Instrum. Methods Phys. Res., 212, 319
Hillas, A. M. 1985, in Proc. 19th Int. Cosmic Ray Conf. (La Jolla), 3, 445
Hillas, A. M., et al. 1998, ApJ, 503, 744
Holder, J., et al. 2003, ApJ, 583, L9
Horan, D., et al. 2002, ApJ, 571, 753
Jarrett, T. H., Chester, T., Cutri, R., Schneider, S. E., & Huchra, J. P. 2003, AJ, 125, 525
Konopelko, A., et al. 1999, in Proc. 26th Int. Cosmic Ray Conf. (Salt Lake City), 3, 426
Krennrich, F., et al. 1999, ApJ, 511, 149
———. 2001, ApJ, 560, L45
———. 2002, ApJ, 575, L9
———. 2003, in Proc. 28th Int. Cosmic Ray Conf. (Tsukuba), 5, 2603
LeBohec, S., & Holder, J. 2003, Astropart. Phys., 19, 221
Mohanty, G., et al. 1998, Astropart. Phys., 9, 15
Nikishov, A. I. 1962, Soviet Phys.—JETP, 14, 393
Nilsson, K., Pursimo, T., Takalo, L. O., Sillanpää, A., Pietilä, H., & Heidt, J. 1999, PASP, 111, 1223
Nishiyama, T., et al. 1999, in Proc. 26th Int. Cosmic Ray Conf. (Salt Lake City), 3, 370
Patnaik, A. R., Browne, I. W. A., Wilkinson, P. N., & Wrobel, J. M. 1992, MNRAS, 254, 655
Perlman, E. S., et al. 1996, ApJS, 104, 251
Petry, D., et al. 1996, A&A, 311, L13
———. 2002, ApJ, 580, 104
Punch, M., et al. 1992, Nature, 358, 477
Quinn, J., et al. 1996, ApJ, 456, L83
Reynolds, P. T., et al. 1993, ApJ, 404, 206
Schroedter, M. 2004, Ph.D. thesis, Univ. Arizona
———. 2005, ApJ, 628, 617
Stecker, F. W. 1999, Astropart. Phys., 11, 83
Stevens, J. A., & Gear, W. K. 1999, MNRAS, 307, 403
Tluczykont, M., et al. 2003, in Proc. 28th Int. Cosmic Ray Conf. (Tsukuba), 5, 2547
Urry, C. M., Scarpa, R., O'Dowd, M., Falomo, R., Pesce, J. E., & Treves, A. 2000, ApJ, 532, 816
Weekes, T. C., Lamb, R. C., & Hillas, A. M. 1987, in Very High Energy Gamma Ray Astronomy, ed. K. E. Turver (NATO ASI Ser. C, 144; Dordrecht: Reidel), 235
Weekes, T. C., et al. 1989, ApJ, 342, 379
White, R. L., & Becker, R. H. 1992, ApJS, 79, 331
Xie, G. Z., Zhou, S. B., Dai, B. Z., Liang, E. W., Li, K. H., Bai, J. M., Xing, S. Y., & Liu, W. W. 2002, MNRAS, 329, 689